View metadata, citation and similar papers at core.ac.uk
brought to you by CORE
provided by NASA Technical Reports Server

34-17
J72320
148

TDA Progress Report 42-100

N90-21884

February 15, 1990

Galileo Earth Approach Navigation Using Connected-Element Interferometer Phase-Delay Tracking

S. W. Thurman
Navigation Systems Section

This article investigates the application of a Connected-Element Interferometer (CEI) to the navigation of the Galileo spacecraft during its encounter with Earth in December 1990. A CEI tracking demonstration is planned for the week of November 11 through 18, 1990, from 27 days to 20 days prior to Earth encounter on December 8. During this period, the spacecraft will be tracked daily with Deep Space Network Stations 13 and 15 at Goldstone. The purpose of this work is twofold: first, to establish and define the navigation performance expected during the tracking demonstration and, second, to study, in a more general sense, the sensitivity of orbit determination results obtained with CEI to the data density within CEI tracking passes and to important system parameters, such as baseline orientation errors and the phase-delay measurement accuracy. Computer simulation results indicate that the use of CEI data, coupled with conventional range and Doppler data, may reduce the uncertainty in the declination of the spacecraft's incoming trajectory by 15 to 66 percent compared with the operational solution using range and Doppler data only. The level of improvement depends upon the quantity and quality of the CEI data.

I. Introduction

Connected-Element Interferometry (CEI) is being developed for use as a medium-accuracy (100–400 nrad for individual measurements) angular measurement system [1]. The use of a common frequency reference distributed through a fiber-optic link to two nearby antennas would be used to make very precise measurements of the phase delay of signals from a radio source. Since the measurements are made at a single frequency, there is no need for a transponder on board the spacecraft for beat frequency generation, as required for wideband Δ Very Long Baseline Interferometer (ΔVLBI) observations. The incoming data from each station are routed through the fiber-optic link to an on-site correlator, whose output data will then be sent immediately to JPL to be processed, along with other radio metric data, for navigation use.

The principal advantages of CEI over the present intercontinental ΔVLBI system are the simplicity of the measurement system and the speed with which the data become available for use. The long observation periods which can be obtained with two nearby antennas and the

near-real-time correlation of the incoming signals make CEI very attractive for use as a navigation tool. With CEI, it is possible to monitor system performance as the measurements are being made and to take corrective action if problems occur. The combination of many CEI measurements made over a single tracking pass make it possible to achieve angular measurement accuracies on the order of 50 nrad, which should be very useful in deep-space navigation.

This article is an expansion and continuation of earlier work done by D.W. Murrow.[1] It begins with a short description of Galileo's approach to its first of two Earth encounters, and continues with a summary of the trajectory, tracking schedule, filter model, and assumed a priori parameter uncertainties used in the orbit-determination simulations which follow. All computer simulations were performed using the Orbit Determination Program (ODP) system software. The results of Murrow's earlier study are summarized, and are used as a basis for comparison and contrast with the new simulations which follow.

II. Galileo Earth Gravity Assist One (EGA1)

This study was performed using a prelaunch reference trajectory, in which it was assumed that the spacecraft was injected into its interplanetary trajectory on October 10, 1989. The Galileo EGA1 trajectory segment begins shortly after the spacecraft's encounter with Venus on February 9, 1990. Navigation accuracy during this time frame with two-way range and Doppler data is degraded due to the near-zero declination of the incoming trajectory, shown in Fig. 1. In addition, there are several targeting maneuvers during the approach which must be determined very accurately to meet mission requirements. The low declination of the flight path leads to a large uncertainty in the declination component of the targeting conditions, expressed in B-plane coordinates.[2] In the CEI tracking demonstration, data will be taken for one week, using the baseline formed by Deep Space Stations (DSSs) 13 and 15 at Goldstone, from encounter −27 days (E−27) to E−20 days (November 11–18, 1990), spanning one of the targeting maneuvers scheduled for E−25 days. CEI passes will be made daily during this time, using quasar P0528+134 to create an observable consisting of the phase delay from the spacecraft differenced with the phase delay from the quasar. The quasar location relative to Galileo's flight path is also shown in Fig. 1. The DSS 13 to DSS 15 baseline is about 20 km long, with a nearly north-south orientation, and should provide strong information in declination, improving the uncertainty in this component over that obtained with range and Doppler tracking.

[1] D.W. Murrow, "Galileo Earth Approach Analysis Using Connected Element Interferometry Data," JPL IOM GLL-NAV-89-28 (internal document), Jet Propulsion Laboratory, Pasadena, California, February 21, 1989.

[2] "Galileo Navigation Plan," Galileo Project Document 625-566, Revision A (internal document), Jet Propulsion Laboratory, Pasadena, California, October 1989.

III. Trajectory

A. Epoch

The epoch is at 1990 February 13 08:44:09.556 (Ephemeris Time). The spacecraft state in Earth-centered Earth mean equator and equinox of B1950.0 Cartesian coordinates is:

$$X = 1.968896282785908 \times 10^7 \text{ km}$$

$$Y = -4.981570235638191 \times 10^7 \text{ km}$$

$$Z = -1.483032488173643 \times 10^7 \text{ km}$$

$$DX = 7.905736580213764 \text{ km/sec}$$

$$DY = -13.48008080659643 \text{ km/sec}$$

$$DZ = -5.834630696184871 \text{ km/sec}$$

The spacecraft's distance and speed with respect to Venus are:

$$R = 2.500 \times 10^6 \text{ km}$$

$$V = 6.363 \text{ km/sec}$$

The spacecraft's distance and speed with respect to Earth are:

$$R = 5.558 \times 10^7 \text{ km}$$

$$V = 16.68 \text{ km/sec}$$

B. Trajectory Correction Maneuver (TCM) Schedule

The schedule for the trajectory correction maneuvers follows.

Maneuver	Time, ET	Nominal Magnitude, m/sec
TCM1	1990 May 11 12:00:00	12.093
TCM2	1990 May 31 12:00:00	0
TCM3	1990 October 09 11:32:10	0
TCM4	1990 November 13 11:32:10	0
TCM5	1990 November 26 11:32:10	0

C. Closest Approach to Earth

The closest approach to Earth occurs on 1990 December 8 11:32:10.586 (ET).

IV. Baseline Tracking Schedule

In Table 1 all data (range, Doppler, and CEI) are assumed to be at S-band (2.29 GHz) frequency. The simulations use all data up to November 22, 1990, the data cutoff point for the EGA1 navigation delivery. In this study, simulated CEI data are taken with the DSS 13 to DSS 14 baseline, although the actual CEI demonstration will be performed using the DSS 13 to DSS 15 baseline. DSS 14 and DSS 15 are very near each other (200 m apart) at the Goldstone complex, so the results presented in Table 1 are equally valid for both stations.

V. Filter Model and Assumed A Priori Parameter Uncertainties

The parameter list described here is based primarily on the orbit-determination error model used by the Galileo Project.[3] Range and Doppler data taken by DSS 14 (Table 1) were removed from the filter for the CEI simulations to avoid creating over-optimistic results. The baseline orientation uncertainty for the DSS 13 to DSS 14 baseline was not modeled explicitly in most of the simulations, but was accounted for in some sense by quasar-direction uncertainty. There were some cases, described in Section VI, in which station-location errors were assumed for DSSs 13 and 14. In these cases, station coordinates for DSS 13 and DSS 14 were included as "consider" parameters—parameters which influence the uncertainty in the knowledge of the estimated parameters, but are not estimated themselves.

A. Filter Type

The filter is a batch-sequential epoch state filter with a five-day batch size. The batch size is shorter for certain time periods near maneuvers.

B. Estimated Parameters

The estimated parameters are:

(1) Spacecraft epoch state vector

(2) Three components for each TCM occurring during the data arc—includes TCMs 1, 2, 3, and 4

(3) Radial (with respect to the Sun) solar radiation pressure coefficient (GR)

(4) Radial (with respect to the Earth) bias acceleration

(5) Radial (with respect to the Earth) stochastic acceleration with an assumed time constant of five days ($ATAR$)

C. Considered Parameters

The considered parameters are:

(1) Mass of the Earth ($GM3$)

(2) Earth's ephemeris

(3) Transverse (with respect to the Sun) solar radiation pressure coefficients (GX and GY)

(4) Station coordinates for DSS 43 and DSS 63

(5) Wet troposphere component at DSSs 43 and 63

(6) Dry troposphere component at DSSs 43 and 63

(7) Daytime ionosphere at DSS 43 and DSS 63

(8) Nighttime ionosphere at DSS 43 and DSS 63

(9) Quasar direction uncertainty (right ascension and declination)

D. A Priori 1σ Uncertainties for Estimated Parameters

(1) Spacecraft epoch state:
position components: 1.0×10^8 km
velocity components: 1.0×10^8 km/sec

(2) Trajectory correction maneuvers per component:
TCM1: 12.0 cm/sec
TCM2: 10.0 cm/sec
TCM3: 10.0 cm/sec
TCM4: 10.0 cm/sec

(3) Radial solar radiation pressure coefficient: $\sigma_{GR} = 0.17 = 10\%$ of nominal value of GR

(4) Radial bias acceleration: 1.0×10^{-12} km^2/sec^4

(5) Radial stochastic acceleration: $\sigma_{ATAR} = 1.0 \times 10^{-12}$ km^2/sec^4, time constant $\tau = 5$ days

E. A Priori 1σ Uncertainties for Considered Parameters

(1) Mass of the Earth: $\sigma_{GM3} = 0.14142$ km^3/sec^2.

(2) Earth's Ephemeris: statistics used are from Planetary Ephemeris DE125. The Earth's ephemeris

[3] D. W. Murrow, "Galileo Orbit Determination Error Model Asumptions," JPL IOM GLL-NAV-89-16 (internal document), Jet Propulsion Laboratory, Pasadena, California, February 3, 1989.

uncertainty relative to the Sun, at the trajectory epoch (February 13, 1990) is:

Position:	radial	0.02 km
	along track	20.58 km
	cross track	8.21 km
Velocity:	radial	0.002 mm/sec
	along track	0.058 mm/sec
	cross track	0.870 mm/sec

(3) Transverse solar radiation pressure coefficients: $\sigma_{GX} = \sigma_{GY} = 0.0342$ (2% of nominal value of GR).

(4) Station coordinates consist of a correlated, station-location, error covariance generated by Murrow and Nicholson.[4] Only the sigmas of the diagonal elements are stated.

DSS 43:	radial	0.48 m	DSS 63:	radial	0.47 m
	polar	5.77 m		polar	5.77 m
	long.	0.59 m		long.	0.58 m

(5) Wet troposphere: 4-cm uncertainty at DSS 43 and DSS 63

(6) Dry troposphere: 1 cm

(7) Daytime ionosphere: 75-cm uncertainty at DSS 43 and DSS 63

(8) Nighttime ionosphere: 15 cm, ionosphere uncertainty values quoted are for S-band (2.29 GHz)

(9) Quasar direction uncertainty (right ascension and declination): 100 nrad for each component

F. Measurement Accuracy

All data points used in the simulations were assigned 1σ uncertainties by data type as follows:

(1) Range: 1000 m

(2) Doppler: 0.50 mm/sec (for a 60-sec count time)

(3) CEI: 8.0 mm (400 nrad), 4.0 mm (200 nrad), or 1.0 mm (50 nrad)

VI. Results

The measure of performance used to express the *quality* of each simulated solution consists of three components: two representing the uncertainty in the direction and magnitude of the *impact parameter*, or B-vector, within the B-plane, and the third representing the uncertainty of the third B-plane component, the linearized time of flight (LTOF). These three parameters completely characterize the uncertainty in the targeting of the spacecraft's incoming flight path and its time of closest approach to the Earth.

Figure 2 shows the error ellipses (representing uncertainty in the magnitude and direction of the B-vector) in the B-plane for the four cases generated by Murrow.[5] In this figure, the T-axis lies in the ecliptic plane and is perpendicular to the spacecraft's incoming velocity asymptote (which points into the paper), while the R-axis is perpendicular to both the T-axis and the velocity asymptote, completing an orthogonal coordinate system. In each of the three cases which had CEI data, the CEI points were assumed to be at one-hour intervals, and any points which had a minimum elevation of 15 degrees or less were eliminated. Figures 3, 4, and 5 show breakdowns of the computed and consider-state contributions to the total error uncertainty in each of the three performance measures; the B-vector R-component, the B-vector T-component, and the LTOF, respectively. Table 2 contains a numerical summary of these results.

During its approach, the Galileo spacecraft is flying almost directly at the Earth. An interferometric data type such as CEI will be sensitive to plane-of-sky trajectory deflections (the plane of the sky is the plane perpendicular to the Earth–spacecraft line of sight), and insensitive to along-track perturbations. As shown in Figs. 2, 3, and 4, CEI does indeed have a great deal of impact on plane-of-sky position uncertainty, reflected in the B-plane. Figure 5 shows that the CEI data had no effect on the LTOF uncertainty, as expected. The reduction in the station-location consider error seen in Fig. 3 is likely due to the reduced dependence of the solution on the Doppler data, which are very sensitive to station-location errors. In Fig. 4, CEI data apparently have some negative impact in that they exaggerate the computed error and the media effects on the range and Doppler data, resulting in some degradation in solution accuracy.

An assumed CEI data rate of 1 point/hr during a pass is probably a very conservative estimate of the data rate which can be achieved in practice. In studying the effects of troposphere fluctuations, the dominant error source in CEI

[4] D. W. Murrow and F. T. Nicholson, "Station Location Covariance," JPL IOM GLL-NAV-88-50 (internal document), Jet Propulsion Laboratory, Pasadena, California, September 2, 1988.

[5] D. W. Murrow, "Galileo Earth Approach Analysis Using Connected-Element Interferometry Data," JPL IOM GLL-NAV-89-28 (internal document), Jet Propulsion Laboratory, Pasadena, California, February 21, 1989.

phase-delay measurements, Edwards [2] has shown that successive observations separated by as little as 200–300 seconds should have a correlation coefficient of less than 0.1. The implication is that essentially uncorrelated CEI measurements may be generated as fast as is physically possible, given the capabilities of the current equipment (predicted to be about 300 seconds to perform one observation). It must be pointed out here that much less is known about random fluctuations in the ionosphere, which may have some impact on the degree of correlation between measurements taken at S-band (2.29 GHz).

In the next set of cases, simulations were generated using CEI data rates of 4, 8, and 12 points/hr for each of the measurement accuracies (8 mm, 4 mm, and 1 mm) used previously. Table 3 contains a summary of the results obtained. Figure 6 shows the B-plane error ellipses obtained with data rates of 1, 4, 8, and 12 points/hr for 4-mm (200-nrad) CEI data. Figures 7 and 8 portray the behavior of the B-vector component uncertainties as a function of the CEI data rate for each of the data weights used (1 mm, 4 mm, and 8 mm). Finally, Figs. 9 and 10 give error breakdowns of the B-vector components for the four cases run using 4-mm CEI. The principal effects of adding in more CEI data are reductions in the magnitude of the computed error and the station-location consider error in B·R, as shown in Figs. 9 and 10. The behavior of the error source contributions seen in these two figures is representative of the results obtained for 8-mm and 1-mm CEI as well.

The final set of simulations carried out included station-location errors for DSS 13 and DSS 14 as consider parameters. A correlated station-location covariance was generated for DSS 13 and DSS 14 in the same manner employed by Murrow and Nicholson,[6] such that the resulting matrix contained a 2-cm uncertainty in each baseline component. The absolute coordinate uncertainties were as follows:

DSS 13:	radial	0.43 m	DSS 14:	radial	0.43 m
	polar	5.77 m		polar	5.77 m
	long.	0.58 m		long.	0.58 m

The proximity of the two stations results in identical values of uncertainty for the absolute position coordinates of each station.

A 2-cm baseline component uncertainty corresponds to about 1-μrad orientation uncertainty, which should be achievable once some quasar observations from Goldstone baselines become available. The quasar direction uncertainty of 100 nrad was retained here, even though the actual value is about 20 nrad. This was done to facilitate comparison of the results with those in which baseline component errors were not explicitly modeled, even though some "double-accounting" is admittedly taking place.

Six cases were run using different values of data rate and measurement accuracy, with results given in Table 4. Figures 11 and 12 show a comparison of the results for cases with the same tracking schedule and measurement accuracy, both with and without station-location errors for DSS 13 and DSS 14. Performance degradation was largest for cases with the highest data rate and measurement accuracy. Remarkably, though, the degradation observed was insignificant in virtually all of these cases. The "double-differencing" of the spacecraft phase delay with that of the quasar, coupled with the proximity of the two stations, cancels out station-location errors quite well, making the CEI observations nearly insensitive to baseline errors, at least at the 2-cm level.

The effects of baseline length and orientation errors on the CEI phase-delay measurement can be approximated with the following simple formula, which ignores correlations between the two:

$$\sigma_\tau^2 = (\sigma_B \cdot a)^2 + (B \cdot a \cdot \sigma_\phi)^2$$

where

σ_τ = phase–delay measurement uncertainty (cm)

σB = baseline length uncertainty (cm)

σ_ϕ = baseline orientation uncertainty (rad)

a = spacecraft–quasar angle (rad)

Using this formula, a 1σ baseline length uncertainty of 2 centimeters, coupled with a 1σ orientation uncertainty of 1 μrad and a spacecraft–quasar angle of 3 degrees (a typical value for Galileo and P0528+134), produces a 1σ measurement uncertainty of about 1.5 mm for the DSS 13 to DSS 14 baseline (which is 21.5 km in length). This amount of error only starts becoming significant for the cases with an assumed CEI measurement uncertainty of 1 mm, as seen in Fig. 12. For the range of CEI measurement accuracy investigated here, baseline component errors would probably have to exceed the 5-cm level to have much impact on navigation performance.

VII. Summary

For an assumed measurement accuracy of 200 nrad, the addition of CEI data at one point/hr brings about a

[6] D. W. Murrow and F. T. Nicholas, "Station Location Covariance," JPL IOM GLL-NAV-88-50 (internal document), Jet Propulsion Laboratory, Pasadena, California, September 2, 1988.

40 percent improvement in the encounter targeting uncertainty in declination ($B \cdot T$ direction). If the data rate is increased to 10 to 12 points/hr, the improvement in declination uncertainty may be up to 66 percent, again using 200-nrad CEI. With an assumed measurement accuracy of 400 nrad, the level of improvement in declination uncertainty was 15 to 55 percent, indicating that the information content of the CEI data is significant even at a modest level of accuracy. Some degradation occurred in the in-plane ($B \cdot R$ direction) targeting uncertainty, which was 5 to 25 percent greater than that obtained with range and Doppler data only, depending on the CEI data rate and measurement accuracy used. This degradation is due to the influence of parameters which are not explicitly modeled, but are known to affect the radio metric data used in determining the flight path (consider parameters).

Several simulations were performed to study the effects of baseline length and orientation errors on the navigation performance obtained using CEI. With an assumed 2-cm uncertainty in the three components of the DSS 13 to DSS 14 baseline, the degradation in performance versus the earlier cases with no baseline errors was typically 6 percent or less; the largest degradation observed was 9.6 percent. The absolute station-location errors used were nearly the same as those presently used by the Galileo Project. These results indicate that CEI data are remarkably insensitive to both absolute station-location errors and baseline component errors.

VIII. Conclusions

The CEI phase-delay tracking demonstration with the Galileo spacecraft during its approach to Earth may produce a greatly improved trajectory solution over that which will be used operationally. In the cases studied, the addition of more CEI data by increasing the data rate continued to improve the navigation performance and did not further exaggerate the effects of the consider parameters, which were small for the most part. Simulations which included baseline component uncertainties showed that, at the 2-cm level, these error sources cause no significant degradation in performance. The results as a whole indicate that CEI tracking can improve navigation performance for this trajectory with modest assumptions in measurement accuracy, station-location errors, and quasar direction errors.

References

[1] C. D. Edwards, "Angular Navigation on Short Baselines Using Phase Delay Interferometry," *IEEE Transactions on Instrumentation and Measurement,* vol. 38, no. 2, pp. 665–667, April 1989.

[2] C. D. Edwards, "The Effect of Spatial and Temporal Wet-Troposphere Fluctuations on Connected Element Interferometry," *TDA Progress Report 42-97,* vol. January–March 1989, Jet Propulsion Laboratory, Pasadena, California, pp. 47-57, May 15, 1989.

Table 1. S-band data

Time Period, days	Data Types	Data Rate	DSS
E-298 to E-268	Range Doppler	1 pt/day 1 pt/hr (daily passes)	14, 43, 63 14, 43, 63
E-268 to E-219	Range Doppler	2 pts/wk 2 passes/wk at 1 pt/hr	43 43
E-219 to E-207	Range Doppler	1 pt/day 1 pt/hr (daily passes)	14, 43, 63 14, 43, 63
E-207 to E-70	Range Doppler	2 pts/wk 2 passes/wk at 1 pt/hr	43 43
E-70 to E-58	Range Doppler	1 pt/day 1 pt/hr (daily passes)	14, 43, 63 14, 43, 63
E-58 to E-35	Range Doppler	2 pts/wk 2 passes/wk at 1 pt/hr	43 43
E-35 to E+1	Range Doppler	1 pt/day 1 pt/hr (daily passes)	14, 43, 63 14, 43, 63
E-27 to E-20	CEI	1 pass/day (data rates from Quasar P0528 + 134 1–12 pts/hr)	DSS 13–DSS 14 baseline

Elevation cutoff for all data = 15°
Quasar P0528 + 134: right ascension = 82.03°
declination = 13.49°

Table 2. Results summary for CEI data rate of 1 point/hr

CEI Data Weight, mm	$\sigma B \cdot R$, km	$\sigma B \cdot T$, km	$\sigma LTOF$, sec
(Base Range, Doppler)	14.55	6.20	0.184
8 (400 nrad)	12.54	7.97	0.192
4 (200)	8.7	8.08	0.192
1 (50)	4.39	5.34	0.190

Table 3. Sensitivity of results of CEI data rate

CEI Data Weight, mm	Data Rate, pt/hr	$\sigma B \cdot R$, km	$\sigma B \cdot T$, km	$\sigma LTOF$, sec
8 (400 nrad)	1	12.54	7.97	0.192
8	4	8.98	8.14	0.192
8	8	7.35	8.22	0.191
8	12	6.57	8.14	0.191
4 (200 nrad)	1	8.78	8.08	0.192
4	4	6.07	7.96	0.191
4	8	5.21	7.24	0.191
4	12	4.77	6.55	0.190
1 (50 nrad)	1	4.39	5.84	0.190
1	4	3.41	3.71	0.187
1	8	3.07	3.12	0.185
1	12	2.93	2.89	0.184

Table 4. Navigation performance with CEI baseline errors included

CEI Data Weight, mm	Data Rate, pts/hr	$\sigma B \cdot R$, km	$\sigma B \cdot T$, km	$\sigma LTOF$, sec
8	4	9.06	8.17	0.192
8	12	6.60	8.18	0.191
4	4	6.15	8.03	0.191
4	12	4.82	6.55	0.190
1	4	3.52	3.86	0.187
1	12	3.04	3.16	0.184

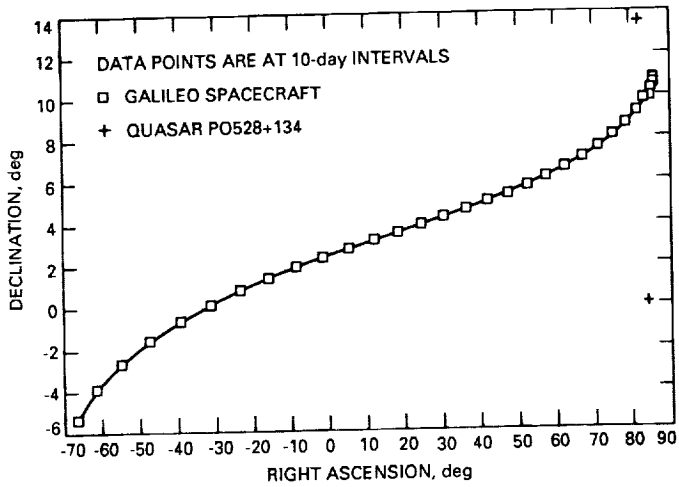

Fig. 1. Galileo EGA1 approach trajectory.

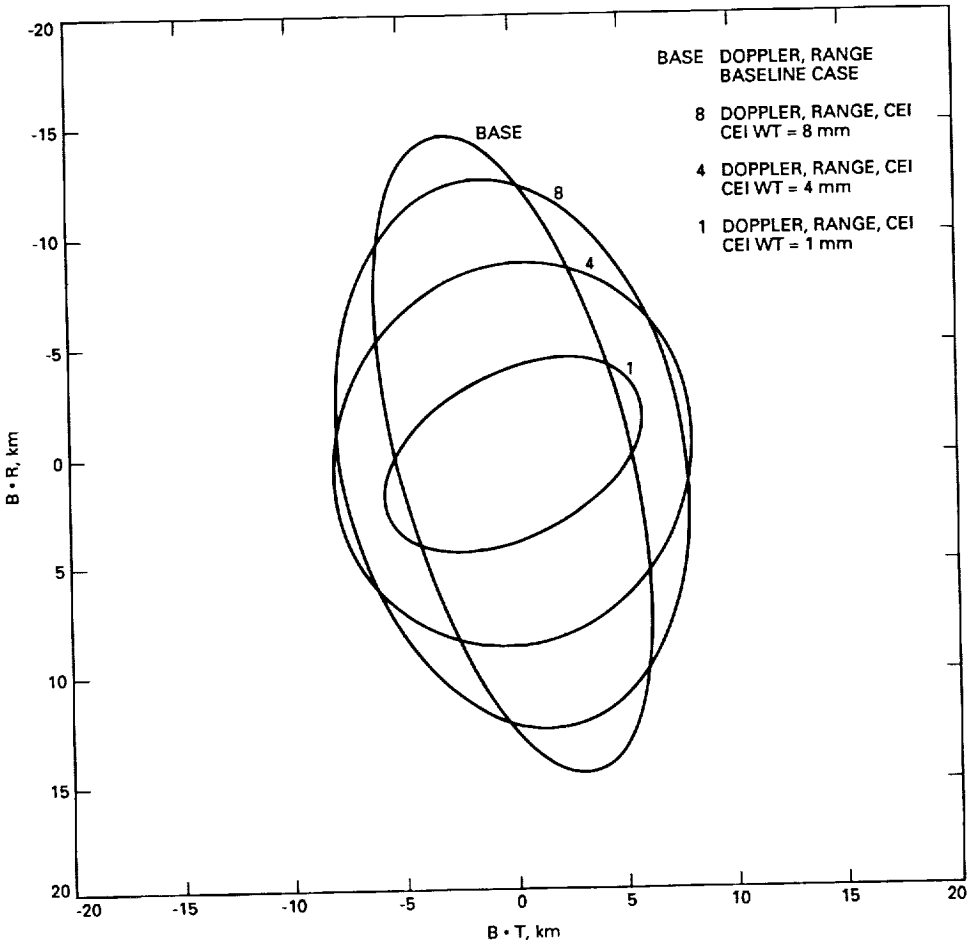

Fig. 2. The B-plane error ellipses for Galileo EGA1 (footnote 5 in text).

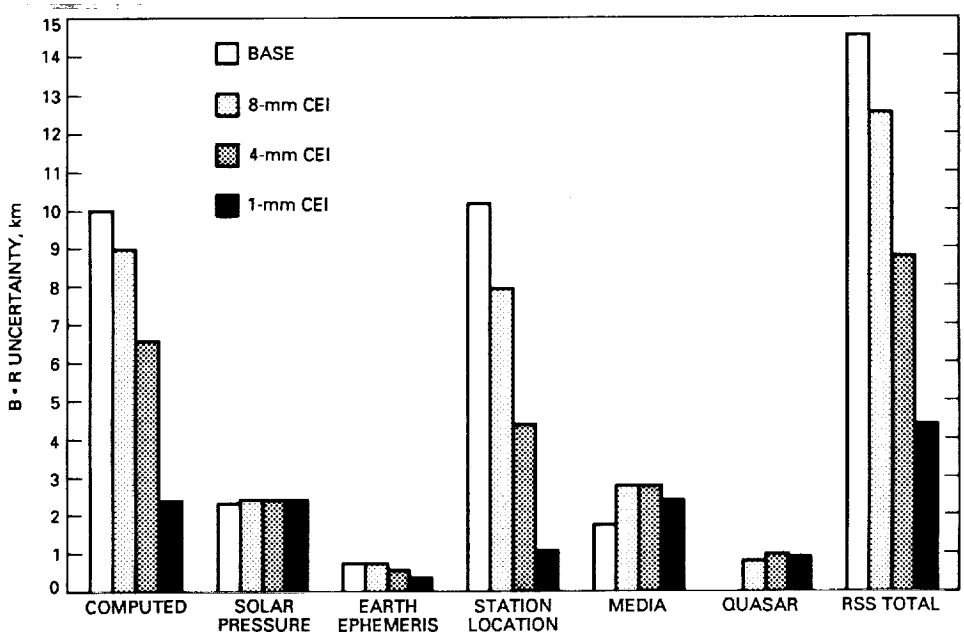

Fig. 3. Error breakdown for B·R component.

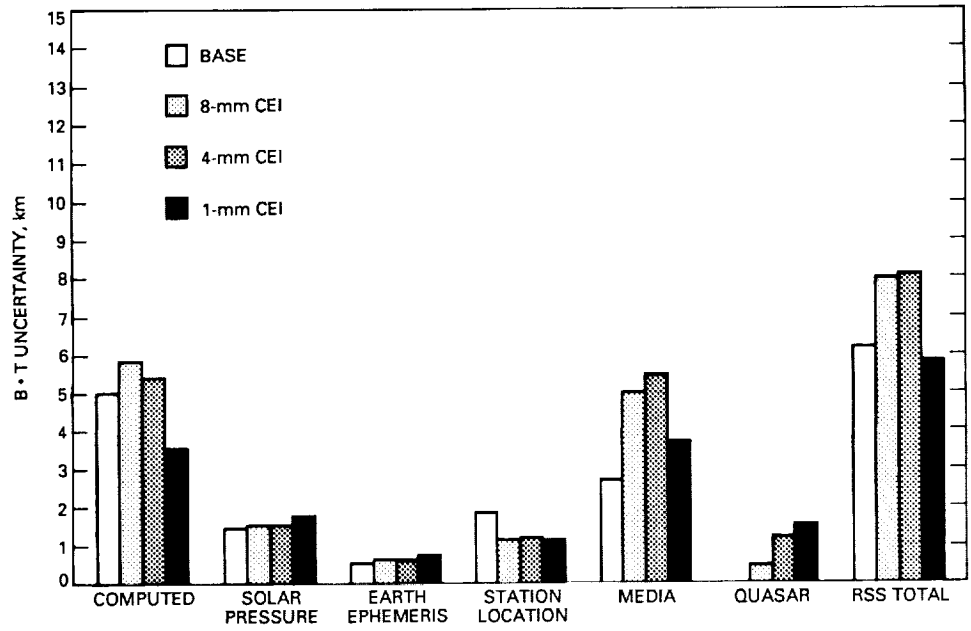

Fig. 4. Error breakdown for B·T component.

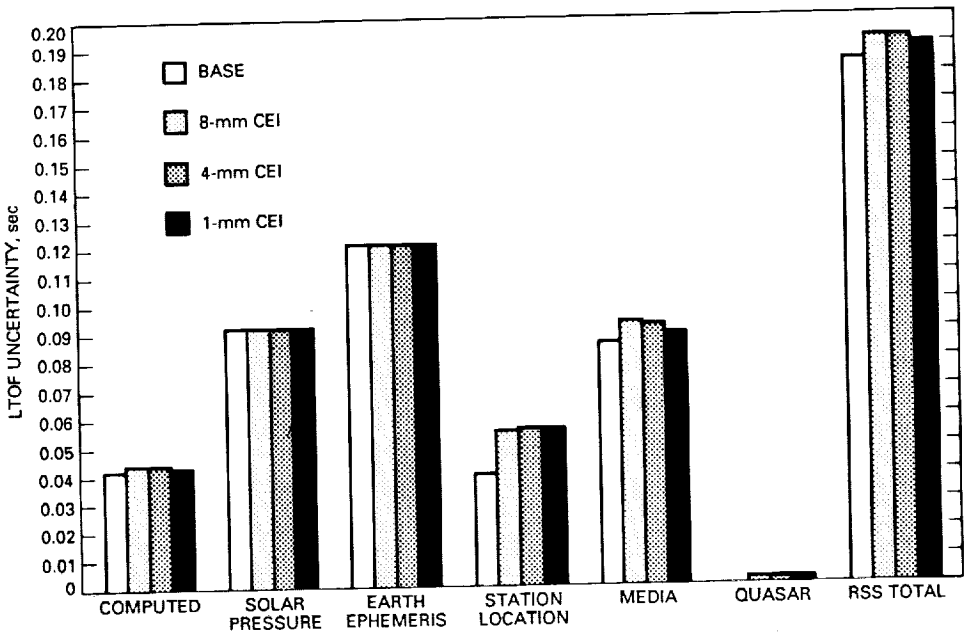

Fig. 5. Error breakdown for LTOF.

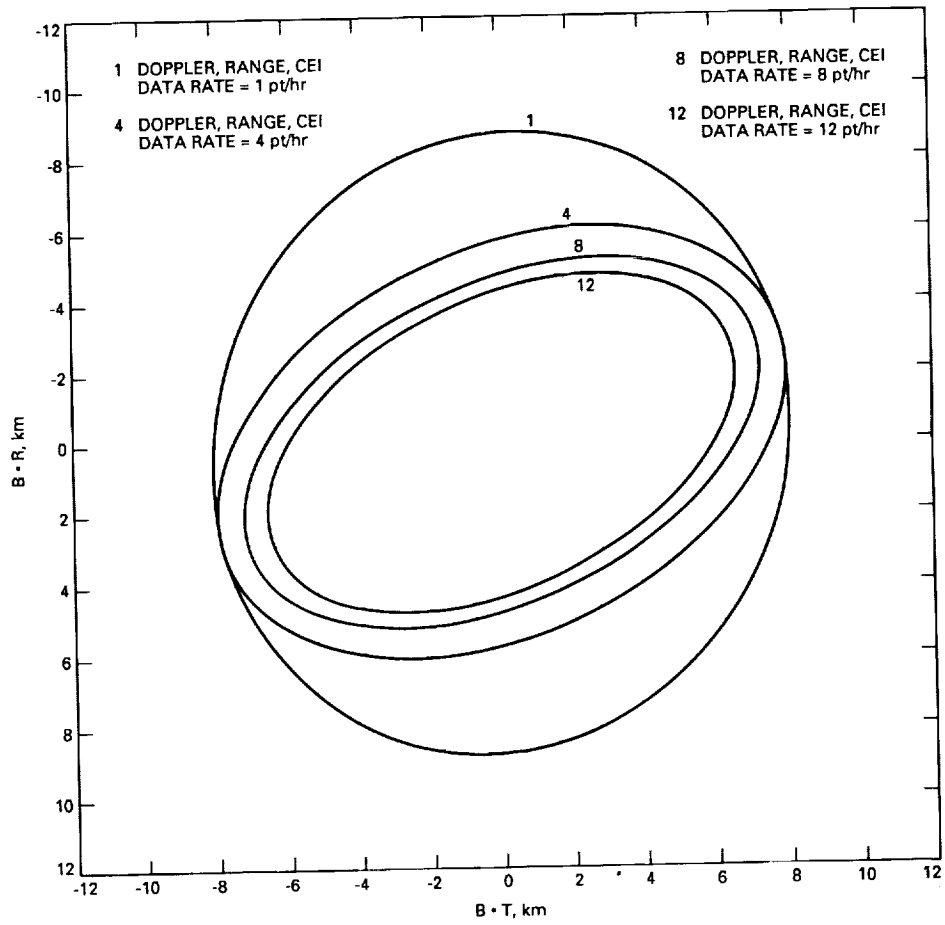

Fig. 6. The B-plane results for different data rates (4-mm CEI).

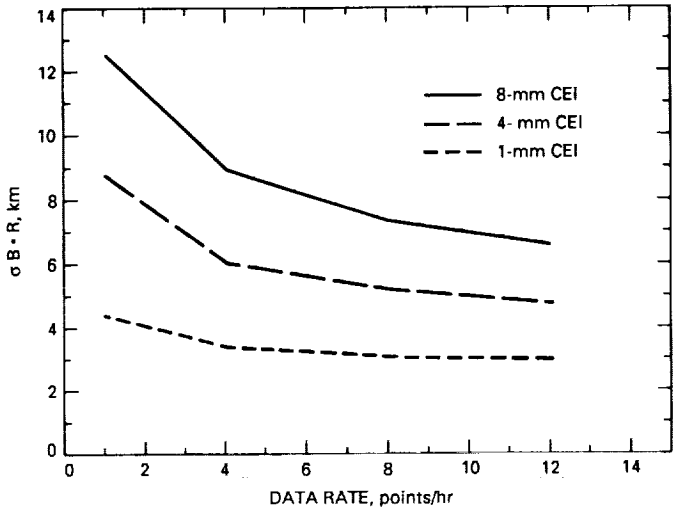

Fig. 7. The B·R uncertainty versus data rate.

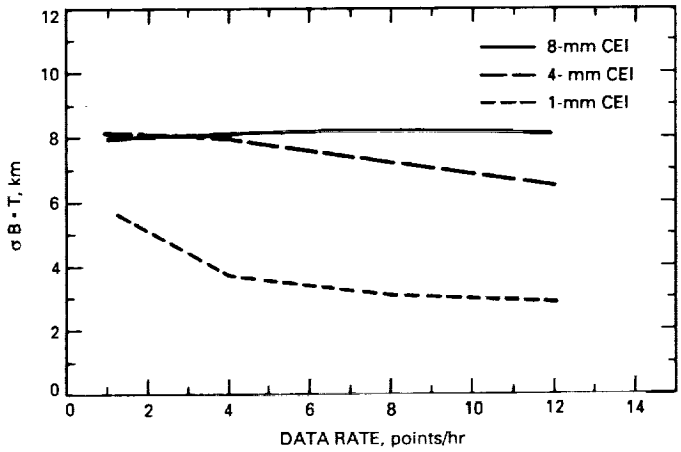

Fig. 8. The B·T uncertainty versus data rate.

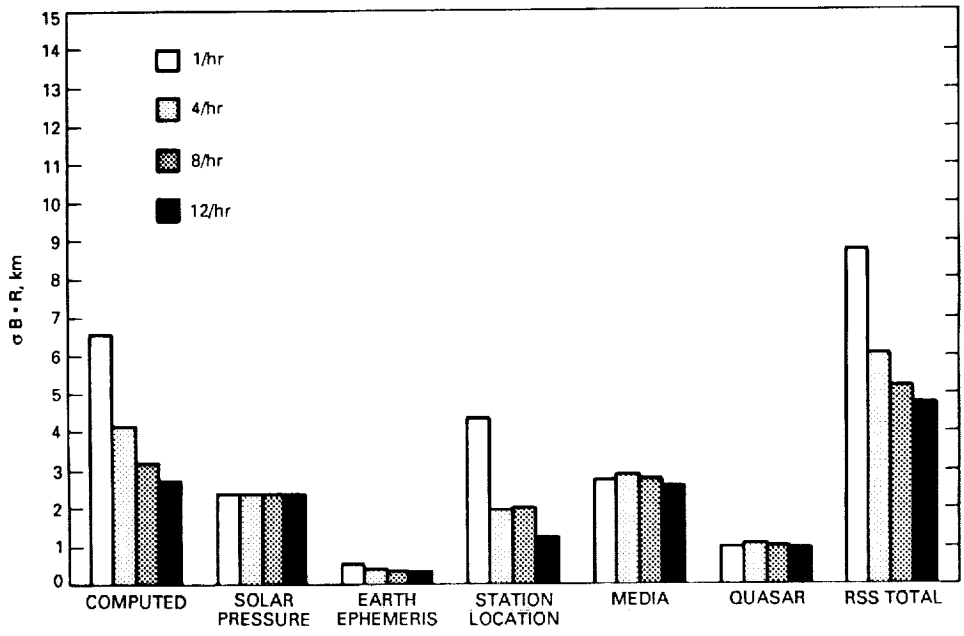

Fig. 9. Error breakdown of B·R for different CEI data rates (using 4-mm CEI).

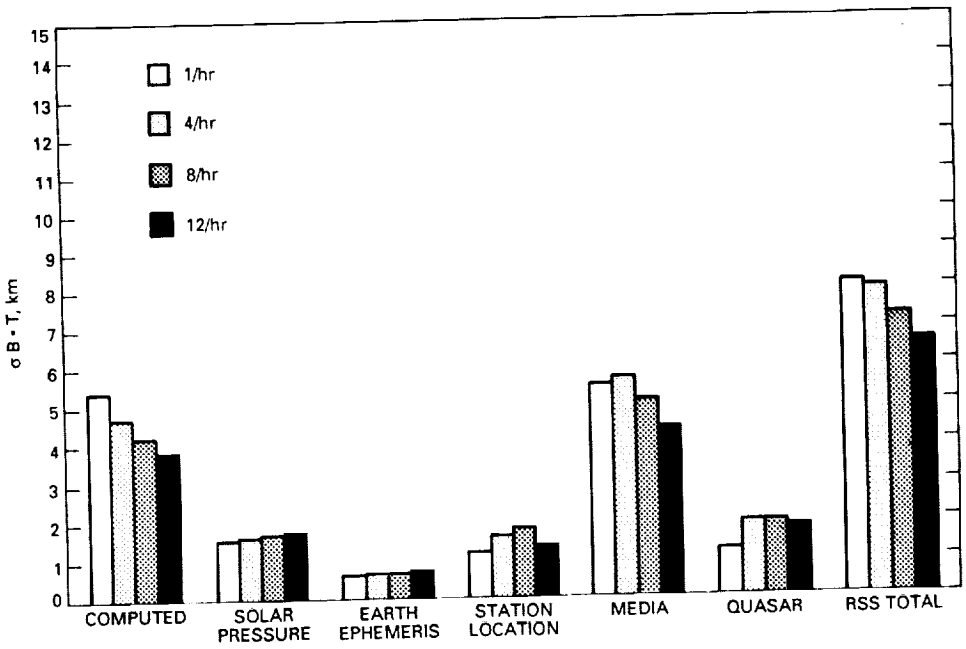

Fig. 10. Error breakdown of B·T for different CEI data rates (using 4-mm CEI).

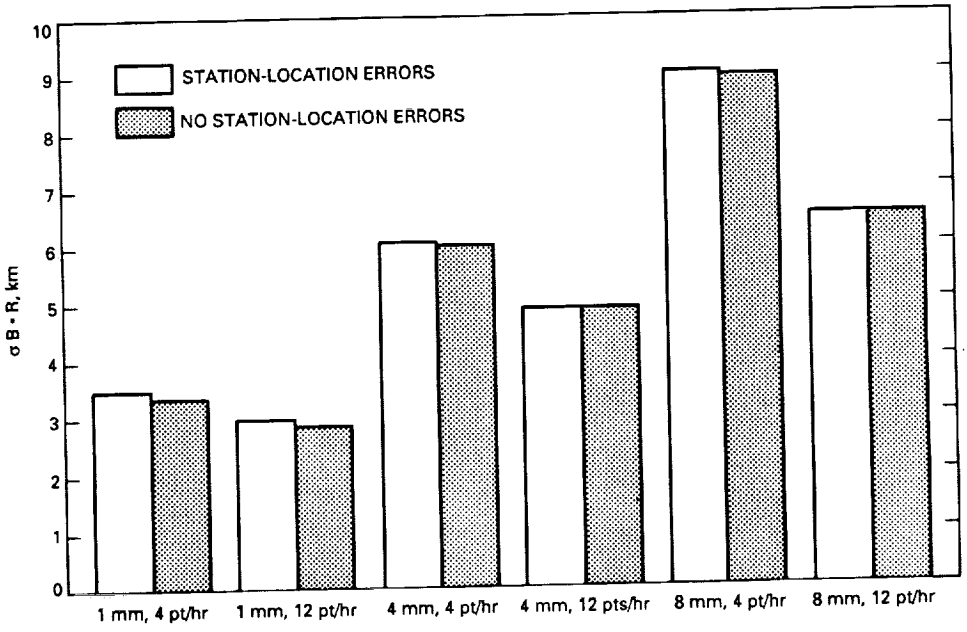

Fig. 11. Performance comparison with station location errors included (B·R component).

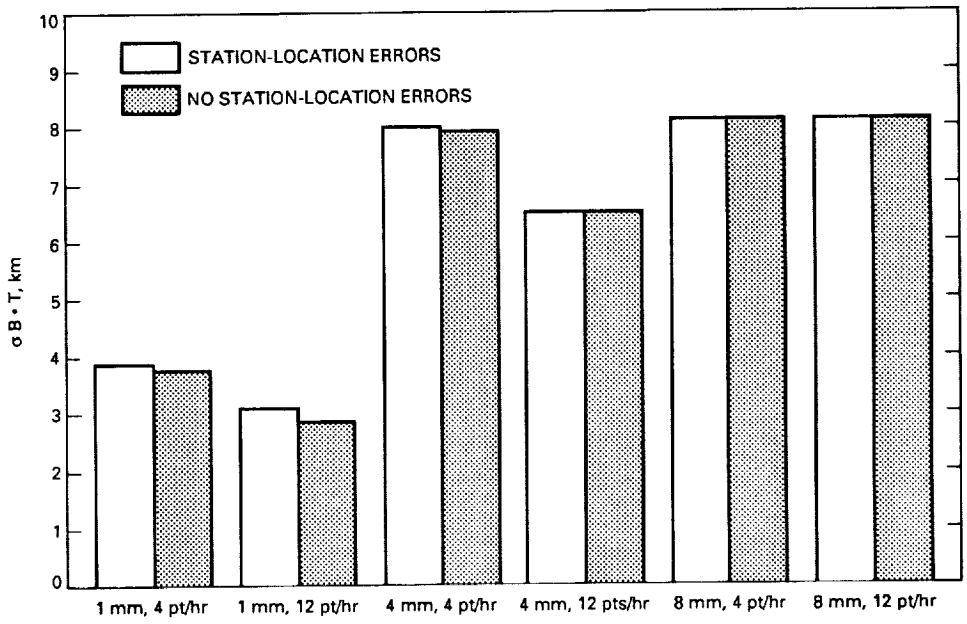

Fig. 12. Performance comparison with station location errors included (B·T component).